Journal of Power Sources 275 (2015) 799–807

Contents lists available at ScienceDirect

Journal of Power Sources

journal homepage: www.elsevier.com/locate/jpowsour

Lithium plating in a commercial lithium-ion battery – A low-temperature aging study

Mathias Petzl [a, *], Michael Kasper [b], Michael A. Danzer [a, b]

[a] Helmholtz-Institut Ulm (HIU), Helmholtzstraße 11, 89081 Ulm, Germany
[b] Zentrum für Sonnenenergie- und Wasserstoff-Forschung Baden-Württemberg (ZSW), Lise-Meitner-Straße 24, 89081 Ulm, Germany

HIGHLIGHTS

- Nondestructive characterization of the degradation effects of lithium plating.
- Capacity retention curves exhibit an inflection point, i.e. maximum aging rate.
- Lithium plating leads to a loss of cyclable lithium which affects the capacity balance.
- Low-temperature plating counteracts its own occurrence during long-term cycling.
- Thickness and area mass of the lithium layer confirm the electrochemical results.

ARTICLE INFO

Article history:
Received 19 August 2014
Received in revised form
23 October 2014
Accepted 11 November 2014
Available online 14 November 2014

Keywords:
Lithium plating
Low-temperature aging
Nondestructive characterization
Cyclable lithium
Cell opening

ABSTRACT

The formation of metallic lithium on the negative graphite electrode in a lithium-ion (Li-ion) battery, also known as lithium plating, leads to severe performance degradation and may also affect the cell safety.

This study is focused on the nondestructive characterization of the aging behavior during long-term cycling at plating conditions, i.e. low temperature and high charge rate. A commercial graphite/$LiFePO_4$ Li-ion battery is investigated in order to elucidate the aging effects of lithium plating for real-world purposes. It is shown that lithium plating can be observed as a loss of cyclable lithium which affects the capacity balance of the electrodes. In this way, lithium plating counteracts its own occurrence during prolonged cycling. The capacity losses due to lithium plating are therefore decreasing at higher cycle numbers and the capacity retention curve exhibits an inflection point. It is further shown that the observed capacity fade is partly reversible. Electrochemical impedance spectroscopy (EIS) reveals a significant increase of the ohmic cell resistance due to electrolyte consumption during surface film formation on the plated lithium. Additional cell opening provides important quantitative information regarding the thickness of the lithium layer and the corresponding mass of the plated lithium.

1. Introduction

The lifetime of Li-ion batteries is crucial concerning their application as energy storage devices in mobile and stationary operation. There are various degradation processes in Li-ion batteries [1–3] which affect performance and durability. It is therefore very important to elucidate the underlying aging mechanisms in order to avoid or mitigate their occurrence. Graphite is the common active material for the negative electrode in Li-ion batteries and it mainly determines the overall aging behavior. The most important degradation mechanisms of the graphite electrode are continuous growth of the solid electrolyte interphase (SEI) and metallic lithium deposition [4].

Lithium plating is different from all other degradation processes in terms of its temperature dependence [5]. It is caused by low-temperature charging with high current and at a high state-of-charge (SOC). However, poor capacity balance can also lead to metallic lithium deposition at higher temperatures. Besides capacity loss and impedance rise lithium plating also presents a serious safety hazard. The metallic lithium can grow dendritically which may cause an internal short circuit of the cell [6–8]. The major aspects of lithium plating in Li-ion batteries are reviewed in Ref. [9], including deposition criteria and different modelling approaches. Intercalation of lithium-ions in the graphite particles and

* Corresponding author.
E-mail address: mathias.petzl@kit.edu (M. Petzl).

http://dx.doi.org/10.1016/j.jpowsour.2014.11.065
0378-7753/

lithium plating on the particle surface are competing during low-temperature charging. High charge currents lead to charge transfer limitation at the particle/SEI interface. Lithium plating occurs when the graphite potential is reduced below 0 V vs. Li/Li^+. However, plating might also be due to mass transport limitation. If the lithium-ion diffusion in the graphite particle is too slow, the particle surface becomes saturated with lithium-ions which consequently leads to lithium plating. These polarization effects are both aggravated with decreasing temperature.

There are a lot of aging studies on commercial Li-ion batteries in the literature which mainly address the performance degradation at ambient or high temperatures due to SEI growth and loss of graphite active material [10–13]. However, the occurrence of lithium plating is only shown as a consequence of cycling in a narrow SOC range [14]. Others assume that lithium plating is the reason for fast performance degradation [15].

In this study lithium plating is forced by low-temperature charging in order to investigate the corresponding aging effects. It is important to note that all other degradation processes and side reactions, e.g. SEI growth, are assumed to be negligible at low temperatures according to the Arrhenius equation [5]. Therefore, lithium plating is the only significant aging process at these cycling conditions. However it must be considered that plated lithium metal induces further degradation due to additional surface film formation and electrochemical isolation of active material.

The investigated commercial Li-ion battery contains $LiFePO_4$ (LFP) as active material of the positive electrode. It is known that LFP is highly durable due to negligible degradation processes [16]. Therefore, the observed aging effects are assumed to be entirely caused by lithium plating and its accompanied processes. LFP also exhibits a very flat voltage profile [17] which simplifies the interpretation of full cell voltage profiles. In detail, all voltage plateaus are due to the phase behavior of the graphite electrode. This is crucial for an unambiguous characterization of the aging behavior by nondestructive electrochemical methods [18–20].

Short-term effects of lithium plating are already known [21,22] and allow for an indirect detection and quantification of this aging process [23]. The operating conditions for lithium plating in the investigated battery were also identified in our previous study [23]. These conditions are applied here in order to characterize the long-term effects of lithium plating on the battery performance. Furthermore, the reversibility of the plating losses is investigated by recovery cycling at higher temperatures. In addition to the electrochemical results, aged cells are opened in different aging states for quantitative information about the plating process. This includes determination of the lithium layer thickness and the mass of the plated lithium metal.

2. Experimental

2.1. Commercial Li-ion battery and electrochemical test equipment

The investigated commercial Li-ion battery is a cylindrical 26650-type cell with 2.5 Ah rated capacity. Like mentioned before, the cell chemistry is based on a graphite (negative electrode) and LFP (positive electrode). This determines the voltage range of 2.0 V–3.6 V, i.e. discharge and charge cutoff voltage. The battery is allowed to be operated down to −30 °C, according to the data sheet.

Electrochemical measurements are performed on a BaSyTec CTS battery test system which is combined with a Gamry G750 card for electrochemical impedance spectroscopy (EIS). All cells are cycled and characterized in an ESPEC climate chamber in order to assure constant and controlled temperature conditions. Temperature equilibration is assumed to be completed after a 10 h rest period.

2.2. Electrochemical aging tests

The aging tests consist of constant current – constant voltage (CCCV) low-temperature cycling at −22 °C. This cyclic aging is interrupted after every 20th cycle for the characterization tests at 25 °C. In detail, CC charging is performed with currents of 1C (2.5 A, corresponding to 1.25 mA cm^{-2}) or C/2 which is followed by a CV phase until the current relaxes below C/20. This determines the full capacity (1.0 SOC). Another SOC value (0.8 SOC) is investigated in order to elucidate the effects of SOC on the aging behavior. 0.8 SOC is performed similar to the full capacity. However, the charging step is stopped at 80% of the full capacity. After charging to the aforementioned SOC values, the cells are completely discharged with C/2. This cycling procedure is repeated after a rest period of 1 h.

The characterization test includes a CCCV capacity measurement with 1C charge/discharge current and C/20 CV phases. Afterwards, an EIS measurement is performed at 0.5 SOC with a frequency range of 10 kHz–10 mHz and an AC-amplitude of C/50. This is followed by a detailed investigation of the voltage profile, i.e. a capacity test with smaller charge/discharge current (C/10). The reversibility of the capacity losses is checked by continued cycling at 25 °C after the low-temperature aging tests.

Two cells are tested for each aging conditions in order to confirm reproducibility. MATLAB is used for data evaluation and signal processing.

2.3. Cell opening and quantitative investigations

Additional cells are cycled at −22 °C with 1C in the full capacity range (1.0 SOC) for the quantitative investigations after cell opening. All cells are completely discharged (multiple discharge steps to 2.0 V with decreasing current) before opening in order to reduce the safety hazard due to metallic lithium. The cells are opened at different aging states in a glove-box under argon atmosphere. Afterwards, pictures of the negative electrode's surface are taken in order to investigate the optical changes due to lithium plating. Separation of the negative electrode layer from the positive electrode and separator layer allows for determination of the graphite electrode thickness by a digital thickness gauge from Mitutoyo. The thickness of the copper current collector (10 μm) can be determined after water exposure which leads to delamination of the active material layers. It must be noted that the current collector is coated on both sides. An unaged cell (0 cycles) without lithium plating serves as a reference, i.e. thickness of the unplated electrode. Thus it is possible to derive the thickness of the lithium layer from measuring the thickness of the complete electrode layer. Thicknesses are measured immediately after taking the pictures in order to avoid significant effects of air exposure. The thickness of each electrode is measured at five different points on the surface for averaging.

Masses of the plated lithium are determined by punching out the negative electrode layer to get circular pieces with an area of 20 cm^2 (both sides). This mass per unit area can be easily translated for the complete cell by knowledge of the total electrode area. It is assumed that the metallic lithium is completely transferred to lithium carbonate by prolonged air exposure. Subsequent oven drying leads to loss of the residual electrolyte. In this way, the mass of the plated lithium can be determined from the differences of the dried area mass compared to the unplated reference cell. Details of the calculation are shown later (Section 3.5.3.). The masses of metallic lithium are determined for the inner and outer part of the jelly roll in order to investigate the distribution of lithium metal in the cell.

3. Results and discussion

3.1. Capacity loss

The capacity loss exhibits an unexpected behavior during long-term cycling. Fig. 1a shows the capacity retention curves for the investigated plating conditions. There is a change in curvature in the capacity retention which means that the capacity loss is reduced at progressed degradation states. This inflection point indicates a decrease of lithium plating as the only aging process at these operating conditions. Furthermore, it seems that the capacity retention approximates a constant value at the end of testing. The reason for this peculiar behavior is discussed in the next section.

It is obvious that current and SOC increase aggravate lithium plating and thus induce stronger degradation. The state-of-health (SOH) can be used for comparison of the aging conditions. According to automotive standards, 80% capacity retention generally indicates the end of life (EOL), i.e. SOH = 0. As can be seen from Fig. 1a, current or SOC increase shifts the EOL to lower cycle numbers and thus shorter lifetime. The investigated low-temperature cycling leads to a lifetime of around 90–140 cycles. A comparable study [16] demonstrates a lifetime of more than 2000 cycles at higher temperature (45 °C). This shows that lithium plating leads to severe performance degradation.

The capacity retention curves (Fig. 1a) are fitted by a mathematical function in order to derive the corresponding aging rates (percentage capacity loss per cycle) which are shown in Fig. 1b. A capacity roll-over, i.e. increasing aging rate, is observed up to a maximum which indicates the inflection point. It is obvious that lithium plating is strongest at this aging state. The roll-over behavior is expected from a high-temperature aging study which addresses lithium plating as self-reinforcing [3]. This is due to the progressive pore clogging by lithium metal and the accompanied surface films. Therefore, the active surface area is reduced which increases the local current densities. However, there must be a counter-effect which leads to a decrease of the aging rate with further cycling. This can only be due to a continuous reduction of lithium plating after the inflection point.

3.2. Characterization of the aging behavior

Qualitative information about the degradation mechanism can be derived from the low-current (C/10) voltage profiles included in the characterization test. Differential analysis of these curves allows for a characterization of the underlying aging cause. In detail, there are two complementary methods which are suitable for different degradation effects. Capacity losses are easily characterized by differential voltage (DV; dV/dQ vs. Q) [18]. In contrast, differential capacity (DC; dQ/dV vs. V) [19] is used for characterization

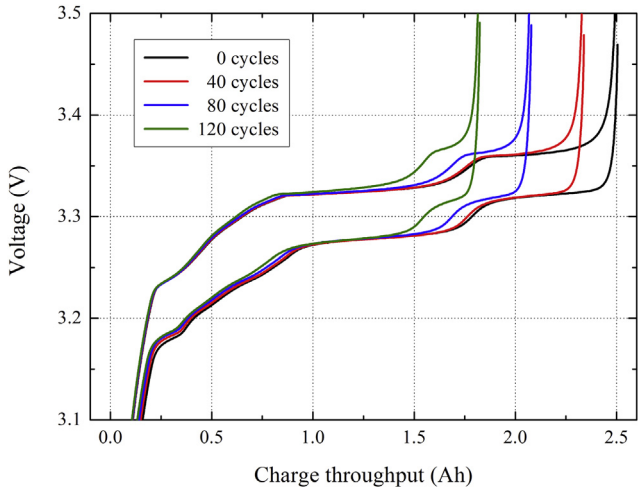

Fig. 2. C/10 voltage profiles at 25 °C with increasing cycle number during low-temperature cycling with 1C/1.0 SOC.

of impedance changes and reaction kinetics during aging. These nondestructive electrochemical methods are applied in many aging studies [10,11,13,15,16].

Correct interpretation of the differential analysis results provides information about the dominant aging mechanism. In general, capacity decrease is due to a (net) loss of cyclable lithium and/or a loss of active material [16]. A loss of cyclable lithium, typically caused by SEI formation, affects the capacity balance of the electrodes. The corresponding capacity loss is due to the fact that the SOC windows of the unaged electrodes cannot be fully utilized anymore. Active material can be lost by electrical isolation of active particles or particle cracking due to volume changes during cycling. Such mechanical degradation is the main reason for active material loss. As a consequence, the operating SOC window of the affected electrode is reduced which is observed as capacity fade.

Fig. 2 shows C/10 voltage profiles for the 1C/1.0 SOC aging condition at various cycle numbers. Degradation is observed as shrinkage of the high-voltage plateau with increasing cycle number. However, the other parts of the voltage profile remain rather unaffected. This means that the observed capacity losses are mostly attained in the high-voltage region. Furthermore, a slight voltage shift can be observed which is due to impedance rise. The following differential analysis elucidates the origin and effects of these characteristic features.

3.2.1. Differential voltage analysis

The DV curves of the discharge voltage profiles (Fig. 2) are depicted in Fig. 3a. DV reflects the slope of the voltage profiles and

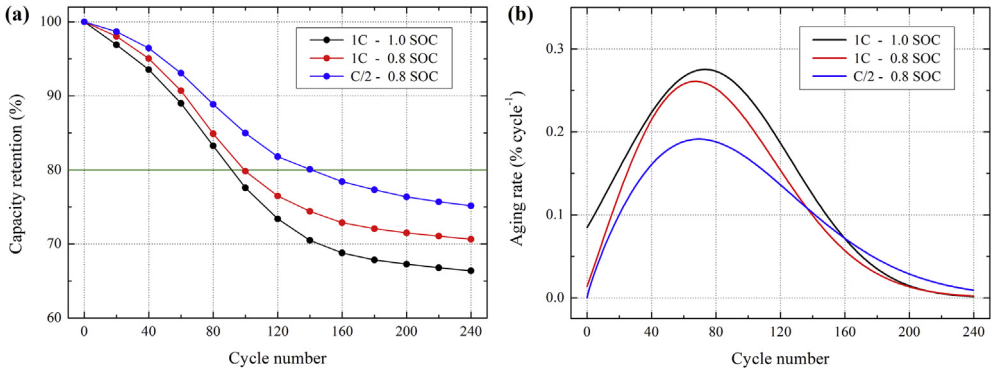

Fig. 1. (a) Capacity retention curves for low-temperature cycling at −22 °C with the different charge currents and SOC ranges. (b) Corresponding aging rates.

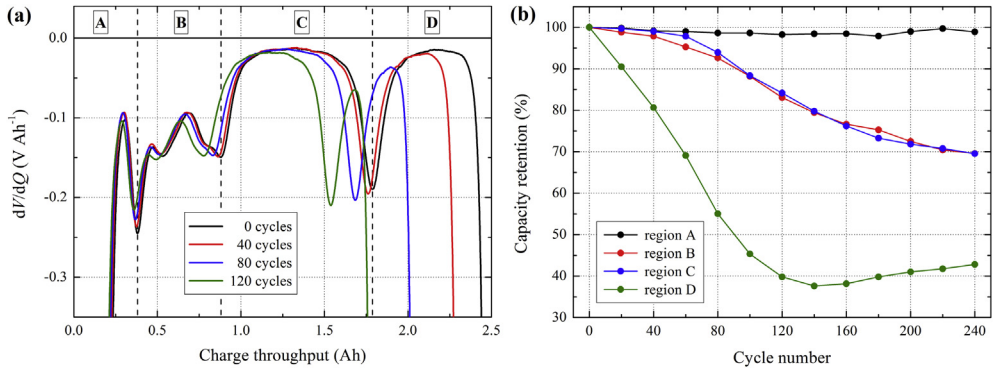

Fig. 3. (a) DV curves of the discharge voltage profiles in Fig. 2. (b) Capacity retention curves of the four regions (A–D).

thus provides important information about the electrodes' phase behavior. As mentioned before, contributions of the positive LFP electrode are negligible due to a very flat voltage profile. Therefore, all observed peaks and features are caused by the graphite electrode and the corresponding degradation processes. The DV peaks are due to the intercalation stages of graphite, i.e. peaks indicate phase transitions between the different graphite intercalation phases [24] according to Gibbs' phase rule.

Further analysis of the aging behavior is achieved by dividing the DV curves into four regions (A-D) [16]. Fig. 3b shows the corresponding capacity retention of these regions, i.e. the capacity loss of the different intercalation stages with increasing lifetime. It is obvious that the high-voltage region D exhibits the strongest capacity loss. The regions B and C show a much smaller decrease, whereas region A remains almost unaffected by low-temperature cycling. This behavior, i.e. the significant capacity loss of region D, is characteristic for a loss of cyclable lithium. Lithium is lost by exfoliation of plated lithium and the formation of surface films. Exfoliated lithium has lost its electrical contact with the graphite electrode and is therefore electrochemically inactive, i.e. “dead” lithium. However, it remains chemically active which leads to further reactions with the electrolyte and thus electrolyte degradation. Electrically isolated lithium may also penetrate through the separator which is an additional safety risk. The capacity recovery of region D after 160 cycles can be interpreted as a reactivation of plated lithium which has not been consumed by reaction with the electrolyte, i.e. recovery of cyclable lithium. This is possible by chemical intercalation of reversibly plated lithium [23,25] which remains electrochemically active due to its electrical contact with the negative electrode matrix. As mentioned above, there are no other aging processes at these operating conditions. However, the similar capacity fade of region B and C can be attributed to a loss of active material. In general, active material loss is observed as an equivalent and simultaneous capacity loss of all regions. Lithium plating causes a loss of active material due to persistent volume stresses. In detail, continuous plating/stripping and surface film formation on the graphite particles cause volume changes in the electrode structure which lead to particle breaking and contact losses due to binder breaking. Active material particles become electrically isolated if the electrode matrix cannot accommodate the additional volume stress caused by the continuous plating and dissolution of metallic lithium. This degradation effect is also known as particle disintegration.

The peculiar capacity behavior, i.e. the inflection point of the capacity retention curves (Fig. 1a), can now be explained by the loss of cyclable lithium as the most prominent degradation effect of lithium plating. Loss of cyclable lithium leads to a perturbation of the cell's capacity balance which means that the operating SOC windows of the electrodes are shifted against each other [26]. This leads to severe capacity losses at the beginning of low-temperature cycling. As mentioned above, the roll-over behavior is due to the self-reinforcing effects of lithium plating (e.g. pore clogging). The shift of the capacity balance increases due to the continuous loss of cyclable lithium. However, the capacity fade and the aging rate start to decrease after a certain time which is observed as an inflection point. This means that lithium plating is reduced and finally ceased with further cycling. It is important to note here that lithium plating only occurs if the graphite potential falls below the potential of metallic lithium (0 V vs. Li/Li$^+$). Therefore, the shift of the operating SOC windows must reach a point where the graphite potential is not reduced too far below lithium potential at the end of CC charging. In other words, the time during which the graphite potential is negative vs. Li/Li$^+$ decreases with cycling. The capacity losses due to lithium plating are continuously decreased in this way. Constant capacity retention at the end of testing means that the graphite potential remains positive vs. Li/Li$^+$ during cycling, i.e. no further lithium plating occurs.

To summarize, the loss of cyclable lithium is the main effect of lithium plating and changes the electrodes' capacity balance in a way that the plating process is reduced or terminated. This is the counter-effect to the expected capacity roll-over. Therefore, lithium plating counteracts itself during prolonged cycling at low temperatures. It is thus assumed that cells at this aging state only exhibit minor capacity fade during low-temperature operation.

3.2.2. *Differential capacity analysis*

DC provides additional information about the degradation effects of lithium plating. Fig. 4a shows the DC curves of the low-current voltage profiles (Fig. 2). Positive and negative DC values denote the charge and discharge direction, respectively. The significant capacity loss of the high-voltage plateau is observed as a reduction of the high-voltage DC peaks for both charging and discharging. This also indicates a loss of cyclable lithium as the high-voltage peaks exhibit a much stronger decrease than the other prominent peaks at lower voltage. The complete loss of the high-voltage charge peak means that the intercalation stage I of graphite (LiC_6, i.e. full charge) is not accessed anymore which leads to an increase of the graphite potential of about 100 mV vs. Li/Li$^+$ [24]. This is due to the shifted capacity balance of the electrodes, i.e. the high SOC region of the graphite electrode is no longer available. Lithium plating is therefore significantly reduced or completely stopped at this point.

DC is also suitable for the investigation of impedance changes. The high-voltage DC peak is shifted to higher voltages in charge direction and to lower voltages in discharge direction, as can be seen from Fig. 4a. This is caused by an impedance rise during low-

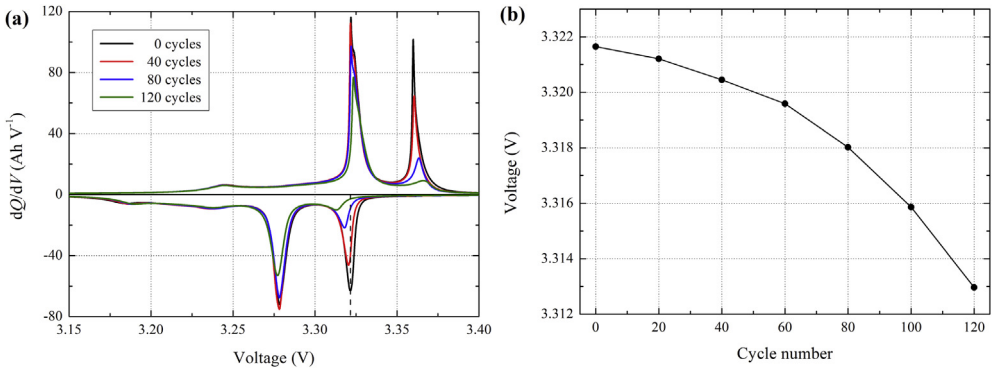

Fig. 4. (a) DC curves of the voltage profiles in Fig. 2. (b) Negative shift of the high-voltage discharge peak.

temperature cycling. Fig. 4b shows the exponential shift of the high-voltage discharge peak. It must be noted that the peak is not identifiable after 120 cycles. The increasing cell impedance is assumed to be due to the layers of metallic lithium and the associated surface films [27]. In general, additional resistive layers lead to an increase of the interphase impedance because of a hindered lithium-ion migration. The impedance behavior is investigated in more detail by EIS in the next section.

3.3. Electrochemical impedance spectroscopy

The reason for the observed impedance rise is further analyzed by EIS investigations. Impedance spectra for increasing cycle number during the 1C/1.0 SOC aging are depicted in Fig. 5a. The most conspicuous change is an increase of the resistance R_0 ($Z'' = 0$) which can be seen as a right shift of the spectra with aging. R_0 is dominated by the ohmic cell resistance which mainly depends on the electrolyte conductivity. The observed resistance increase is therefore due to a reduced ionic conductivity of the electrolyte. This electrolyte degradation is caused by surface film formation on the plated lithium. Electrolyte contact of the lithium metal leads to reduction of electrolyte solvents and thus irreversible consumption. The ionic conductivity is therefore significantly decreased.

Fig. 5b shows the percentage increase of the resistance R_0 for all investigated aging conditions. An almost linear behavior is observed up to 160 cycles. Thus, the continuous lithium plating and corresponding surface film formation lead to an uniform resistance rise. Results of the linear regressions (method of linear least squares) for the first 160 cycles are listed in Table 1. The values of the percentage resistance increase per cycle (ΔR_0) are as expected from the capacity tests. In detail, current and SOC increase lead to faster resistance rise due to enhanced electrolyte degradation (i.e. lithium plating) at these cycling conditions. It must be noted that an increase of the ohmic cell resistance may also cause capacity losses because of the corresponding polarization effects. R^2 is the coefficient of determination which describes the quality of the linear regression. The high values of R^2 support the assumption of a linear behavior.

Table 1
Details of the linear regressions for the increase of R_0 (Fig. 5b) during the first 160 cycles: percentage resistance increase per cycle (ΔR_0) and coefficient of determination R^2 for the different aging conditions.

Aging condition	ΔR_0(%)	R^2
1C-1.0 SOC	0.1087	0.996
1C-0.8 SOC	0.0897	0.9874
C/2–0.8 SOC	0.0689	0.9901

However, there is a flattening of the curves after 160 cycles. This coincides with the capacity retention behavior and the aging rate (Fig. 1). As mentioned above, lithium plating is decreased due to a shift of the cell's capacity balance. This is confirmed by EIS as there is no significant resistance increase without lithium plating and thus no further electrolyte degradation.

3.4. Reversibility

The reversibility of the capacity losses caused by lithium plating is investigated by subsequent cycling at higher temperature (25 °C). Fig. 6a shows the capacity retention curves during normal-

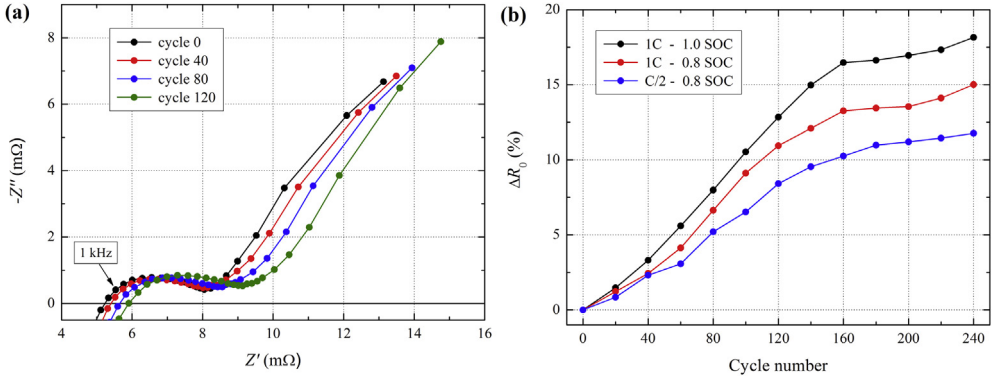

Fig. 5. (a) Electrochemical impedance spectra at 25 °C during low-temperature cycling with 1C/1.0 SOC. (b) Percentage increase of the resistance R_0 for the different charge currents and SOC ranges.

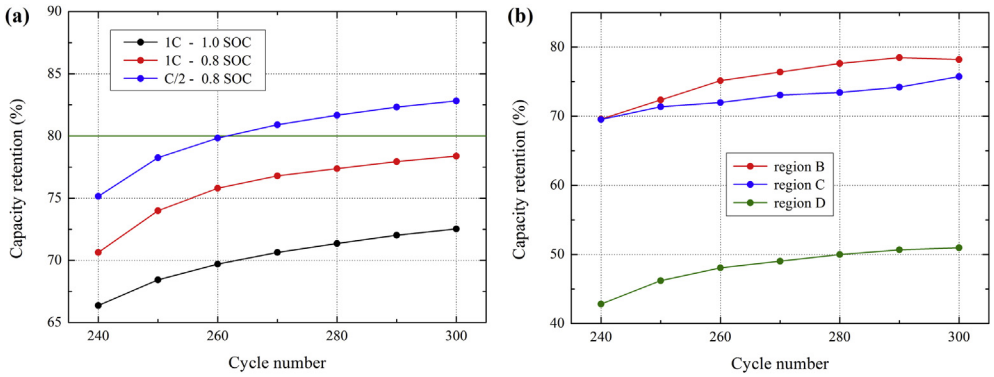

Fig. 6. (a) Capacity retention curves for the different aging conditions during cycling at 25 °C after the low-temperature cycling. (b) Capacity retention curves of the different regions after the low-temperature cycling with 1C/1.0 SOC.

temperature cycling for the different aging conditions. The observed capacity recovery is around 6–9% which means that the capacity losses are reversible to some extent. It is thus possible to revive (SOH > 0) the cell with the highest capacity retention after low-temperature cycling, i.e. the mildest aging conditions. This reversibility shows that some parts of the plated lithium metal and inactive graphite particles are recoverable by temperature increase. Higher temperature leads to enhanced lithium-ion diffusion in the electrolyte and active material particles. The metallic lithium can only be reactivated if there is an electrical contact with the graphite electrode, i.e. reversibly plated lithium. This lithium metal is still electrochemically active in contrast to electrically isolated lithium (exfoliation). The aforementioned chemical intercalation of plated lithium metal is a diffusion process which becomes significant at higher temperatures. Therefore, accelerated lithium-ion diffusion enables partial lithium recovery. The same holds true for the reactivation of a certain amount of graphite particles. The capacity recovery is further analyzed by DV and the corresponding capacity retention curves of the different regions which are shown in Fig. 6b. The similar capacity behavior of the three regions (B–D) indicates that a reactivation of active material (graphite) particles is mainly responsible for the observed capacity recovery. Region A remains almost unaffected and is therefore not shown in the figure.

Furthermore, the reversibility strongly depends on the morphology of the metallic lithium. Morphologies with low specific surface areas exhibit a higher reversibility which is due to a decrease of parasitic side reactions. This is expected for lithium plating at low temperatures in contrast to the lithium deposition at higher temperatures which leads to morphologies with high surface areas (dendritic, mossy-like). Fragile structures like lithium dendrites and moss are much more prone to exfoliation than smooth deposition structures. In addition, the plating morphology can also be affected by an inhomogeneous current distribution.

3.5. Cell opening investigations

The optical and quantitative characterization of the degradation effects is crucial for the confirmation of the nondestructive electrochemical results. Electrochemical investigations are rather qualitative in terms of the real macroscopic effects of aging mechanisms. However, it is possible to derive detailed information about the degradation behavior during the entire lifetime of the cell. In contrast, quantitative results by cell opening are confined to a certain time.

The following (non-electrochemical) investigations provide valuable details about lithium plating which are only attainable by cell opening, i.e. irreversible disassembly of the battery.

3.5.1. Surfaces of the plated negative electrodes

Pictures of the negative electrodes' surfaces at various cycle numbers (1C/1.0 SOC) are shown in Fig. 7. These are taken at air immediately after cell opening in order to avoid reactions with the lithium metal. The electrode surface without lithium plating (0 cycles, reference cell) exhibits a gray color which is due to the graphite active material [28]. There are gradual changes of the electrode surface with increasing cycle number. Lithium metal can be roughly identified by water contact and subsequent gas formation for all cycle numbers besides the reference cell. However, a complete film of metallic lithium is first observed after 80 cycles (Fig. 7d). It is obvious that the lithium metal is uniformly plated and exhibits a silver color. The entire electrode surface is covered with the metallic lithium layer and there are no indications of dendrite formation. This flat and uniform plating is due to the low temperature which alters the electrical and mechanical properties of the inner cell structure. In contrast, local spots and dendrites of lithium metal are expected at higher temperatures.

In addition, the electrode surface seems to be continuously dried out with increasing cycle number. This is consistent with the EIS investigations in terms of the electrolyte consumption due to surface film formation on the metallic lithium. There are no significant changes of the lithium layer up to 120 cycles (Fig. 7f). However, the color of the lithium layer is faded after 160 cycles (Fig. 7g). The formerly uniform metallic layer appears to be thinned and there are points where the gray graphite surface is visible again. This qualitatively confirms that there is no lithium plating at this aging state. It is assumed that parts of the metallic lithium are chemically intercalated [25] during further cycling without lithium plating. This is also indicated by the capacity recovery of region D after 160 cycles in Fig. 3b (Section 3.2.1.). In this way, the amount of lithium metal on the electrode surface is reduced which leads to the observed decrease of the lithium layer thickness.

Quantitative results, i.e. thickness and mass investigations, are shown in the following sections.

3.5.2. Thickness of the lithium layer

Investigation of the cell's thickness behavior is an interesting characterization method which is mainly applicable for pouch cells. This nondestructive technique provides information about the graphite electrode's thickness variation during lithium-ion intercalation and is even used for the detection of lithium plating [29].

In this study, the change of electrode thickness due to lithium plating is measured directly on the electrode level. As described above (Section 2.3.), the thickness of the lithium layer can be determined by referring to the unplated reference cell. Fig. 8 shows the thickness of the lithium layer with increasing cycle number. At

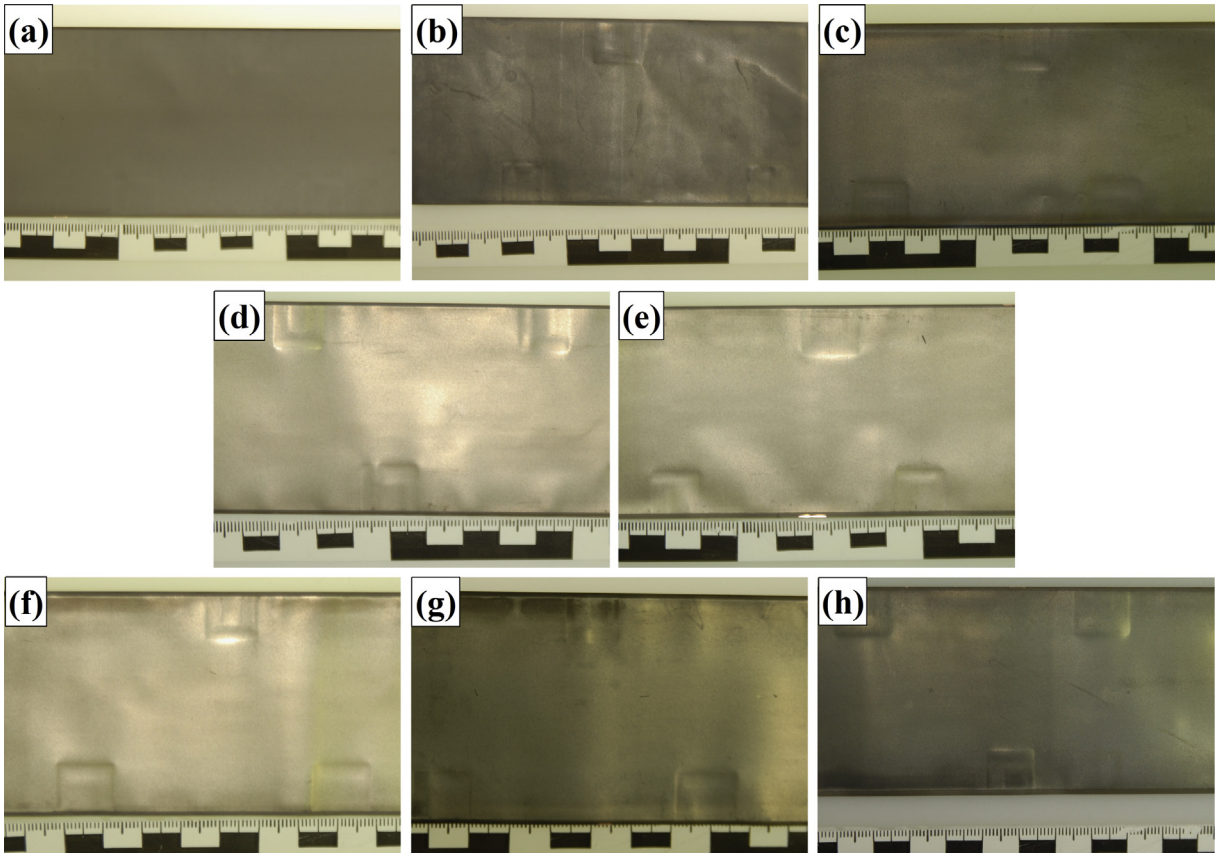

Fig. 7. Pictures of the negative electrodes' surfaces with increasing cycle number during low-temperature cycling with 1C/1.0 SOC: (a) 0 cycles, (b) 40 cycles, (c) 60 cycles, (d) 80 cycles, (e) 100 cycles, (f) 120 cycles, (g) 160 cycles, (h) 200 cycles.

first the layer thickness exhibits a linear increase up to ca. 2 μm at 80 cycles which is followed by a steep rise to the maximum of almost 5 μm at 120 cycles. As can be seen from Fig. 7 (a–c), the first increase occurs without any visible lithium on the electrode surface. It is therefore assumed that lithium is plated in the pores of the graphite electrode (pore clogging) during the first 60–80 cycles. The sharp thickness increase is observed between 80 and 120 cycles where also a complete film of metallic lithium is present on the electrode surface (Fig. 7d–f). Thus, the lithium is plated on the electrode surface during this period of cycling and the actual (pure) lithium layer reaches a thickness of almost 3 μm. Further cycling reduces the thickness of the lithium layer. This observation is in line with what is expected from Fig. 7 (g–h) as the lithium layer seems to be thinned and faded after 160 cycles.

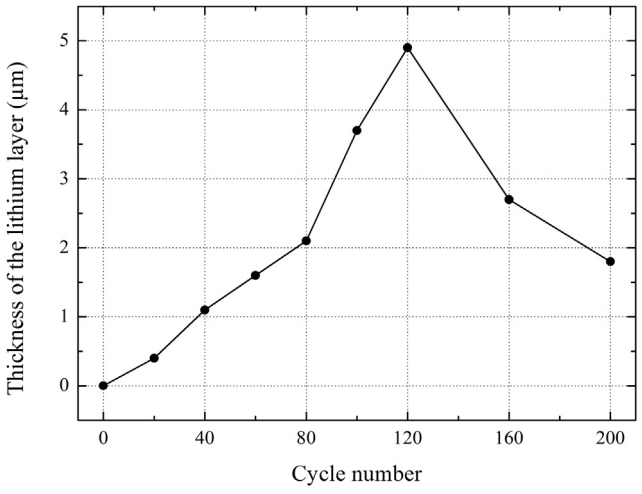

Fig. 8. Thickness of the lithium layer during low-temperature cycling with 1C/1.0 SOC.

The thickness investigations complement and support the assumptions derived from the qualitative optical impressions of the metallic lithium layer. These results are also in accordance with the electrochemical investigations, i.e. capacity retention and impedance behavior.

It is important to note that the presented thicknesses of the lithium layer also include the surface films which are formed on the lithium metal. However, these surface films are assumed to be about 10 nm in thickness [27,30] which is negligible for this investigation.

3.5.3. Area mass of the plated lithium

The area mass of the lithium metal is the most important quantitative information about lithium plating. However, some assumptions are necessary in order to derive meaningful results from this rather simple approach. It is assumed that the plated lithium completely reacts with oxygen to lithium oxide (Li_2O) due to air exposure. The oxide is further transferred to lithium hydroxide (LiOH) and finally lithium carbonate (Li_2CO_3) by reaction with water and carbon dioxide from air. Fig. 9 shows pictures of negative electrode surfaces after oven drying which leads to complete electrolyte evaporation. A white deposit of lithium carbonate is observed on the surface. It seems that more carbonate is formed with increasing cycle number, i.e. higher amount of plated lithium.

The negative electrode of the unplated cell serves as a reference which is only affected by mass reduction due to electrolyte loss. It is

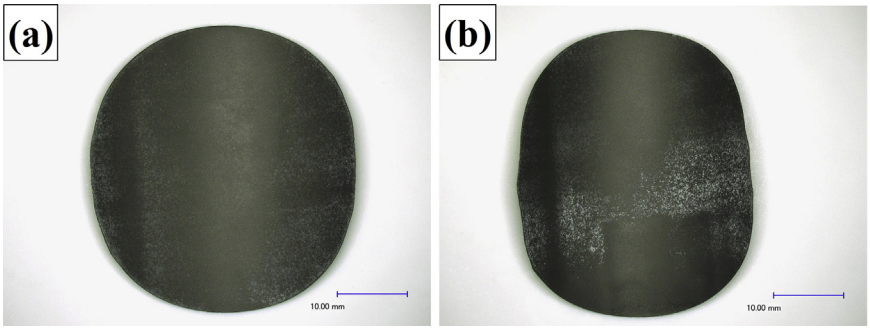

Fig. 9. Pictures of negative electrode surfaces after oven drying: (a) 60 cycles, (b) 100 cycles.

assumed that the amount of evaporated electrolyte is constant. In this way, the mass of the plated lithium can be determined by the mass increase due to the formation of lithium carbonate with regard to the reference cell. Contributions of the relatively thin surface films are assumed to be negligible. Details of the calculation are shown in the following. The amount of carbonate (CO_3^{2-}) $n_{carbonate}$ is calculated from the mass increase $m_{carbonate}$, i.e. $n_{carbonate} = m_{carbonate}/M_{carbonate}$ with the molar mass $M_{carbonate} = 60.01$ g mol^{-1}. According to the chemical formula of lithium carbonate, the mass of the plated lithium m_{Li} is given by $m_{Li} = 2 \cdot n_{carbonate} \cdot M_{Li}$ with $M_{Li} = 6.94$ g mol^{-1}. The corresponding area masses (mg cm^{-2}) are shown in Fig. 10a for the inner and outer part of the jelly roll. An increase of the area mass of lithium is observed up to a maximum at 120 cycles for the inner part of the jelly roll. Further cycling leads to a slight decrease of the area mass which means that there is no additional lithium plating after 120 cycles. The observed decrease is probably due to the chemical intercalation of metallic lithium during prolonged cycling. Therefore, the area mass investigations quantitatively confirm the electrochemical, optical, and thickness results concerning the aging behavior during cycling at plating conditions.

The area mass of lithium in the outer part of the jelly roll exhibits a similar trend. However, the maximum is shifted to 160 cycles which might be due to variations of the internal cell pressure. It is assumed that the mechanical pressure between the electrode layers is higher at the inner part of the jelly roll because of the smaller winding radius. This pressure reduces lithium plating due to mechanical hindrance and changes of the current/potential distribution in the cell, i.e. increase of inhomogeneity. Therefore, the maximum of the area mass of lithium occurs later (i.e. at higher cycle number) for the outer part of the jelly roll. This also explains why the area mass of lithium in the outer part is always higher compared to the inner part, except for the early aging state at 20 cycles. In other words, there is an inhomogeneous distribution of lithium metal in the cell with a higher amount in the outer part of the jelly roll.

Generally, it must be noted that the mechanical effects of metallic lithium in the cell might play an important role for the plating process. According to Fig. 8, the lithium layer reaches 5 μm in thickness which is significant with regard to the thickness of the graphite layer (40 μm). It is thus obvious that the metallic lithium layer affects the mechanical conditions within the cell. Furthermore, there might be a mechanical limit for lithium plating when the cell cannot accommodate additional lithium metal. One possible consequence could be that the metallic lithium is pressed and thus intercalated into the graphite structure.

The geometric surface area of the complete negative electrode is about 2000 cm^2. This enables an estimation of the total mass of plated lithium in the cell per cycle. The averaged mass of the plated lithium per cycle is shown in Fig. 10b. As expected from the above discussion, the mass of plated lithium per cycle is reduced with increasing cycle number. The maximum of about 6 mg per cycle is therefore observed for the first 20 cycles and it is reasonable to assume that this value is even higher for the very first cycle.

4. Conclusions

The presented study elucidates the degradation effects of lithium plating on the negative graphite electrode as the most severe aging process in Li-ion batteries during low-temperature cycling. The observed capacity retention behavior, i.e. decreasing capacity losses at higher cycle numbers, seems peculiar at first. However, nondestructive electrochemical investigations reveal that lithium plating leads to a significant loss of cyclable lithium. This leads to severe capacity fade and also affects the capacity balance of the electrodes which means that the SOC windows are contrarily

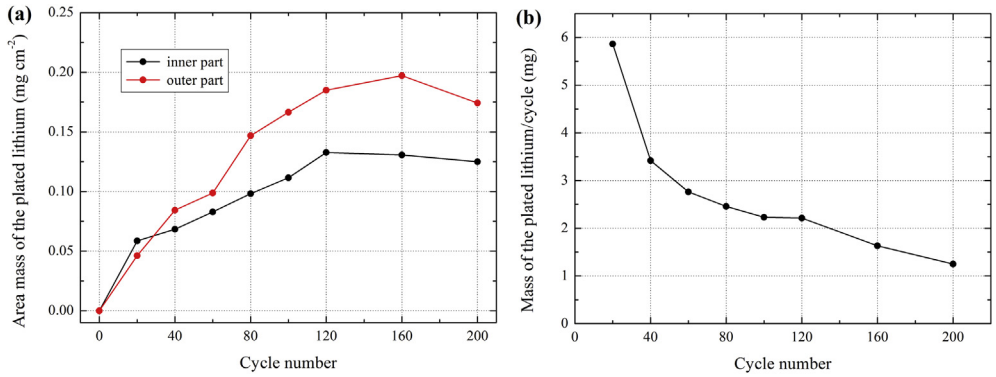

Fig. 10. (a) Area mass of the plated lithium during low-temperature cycling for the inner and outer part of the jelly roll. (b) Averaged mass of the plated lithium per cycle for the complete cell.

shifted. Therefore, lithium plating is gradually reduced due to the fact that the high SOC region of the negative electrode is not electrochemically accessible anymore. The capacity roll-over at the beginning of cycling is thus ceased and the aging rate starts to decrease. This explains the inflection point and the flattening of the capacity retention curves. Thus, it can be concluded that the effects of lithium plating at low temperatures are working against the actual aging cause during long-term cycling. In other words, low-temperature lithium plating is a degradation process which counteracts its own occurrence. As expected, increase of SOC and charge current causes higher capacity fade.

EIS provides the additional information of (ohmic) resistance rise which can be ascribed to the formation of surface films on the plated lithium metal. The electrolyte is consumed and dried out which leads to a decrease of the ionic conductivity.

The electrochemical results are confirmed by cell opening and investigation of the plated graphite electrodes. Determination of the lithium layer thickness and the mass of the plated lithium support the conclusions from the nondestructive investigations. It is further possible to estimate the mass of plated lithium in the complete cell. The mass of plated lithium per cycle is in the same order of magnitude as reported in our previous study [23] based on electrochemical methods.

More generally, this study shows that the aging behavior of Li-ion batteries is at least qualitatively explainable by nondestructive electrochemical investigations.

Acknowledgment

This work was financially supported by the Helmholtz-Institut Ulm (HIU) and the Zentrum für Sonnenenergie-und Wasserstoff-Forschung Baden-Württemberg (ZSW).

References

[1] P. Arora, R.E. White, M. Doyle, J. Electrochem. Soc. 145 (1998) 3647.
[2] J. Vetter, P. Novák, M.R. Wagner, C. Veit, K.-C. Möller, J.O. Besenhard, M. Winter, M. Wohlfahrt-Mehrens, C. Vogler, A. Hammouche, J. Power Sources 147 (2005) 269.
[3] M. Broussely, Ph Biensan, F. Bonhomme, Ph Blanchard, S. Herreyre, K. Nechev, R.J. Staniewicz, J. Power Sources 146 (2005) 90.
[4] V. Agubra, J. Fergus, Materials 6 (2013) 1310.
[5] T. Waldmann, M. Wilka, M. Kasper, M. Fleischhammer, M. Wohlfahrt-Mehrens, J. Power Sources 262 (2014) 129.
[6] R. Bhattacharyya, B. Key, H. Chen, A.S. Best, A.F. Hollenkamp, C.P. Grey, Nat. Mater. 9 (2010) 504.
[7] F. Orsini, A. Du Pasquier, B. Beaudoin, J.M. Tarascon, M. Trentin, N. Langenhuizen, E. De Beer, P. Notten, J. Power Sources 76 (1998) 19.
[8] F. Orsini, A. Du Pasquier, B. Beaudoin, J.M. Tarascon, M. Trentin, N. Langenhuizen, E. De Beer, P. Notten, J. Power Sources 81-82 (1999) 918.
[9] Z. Li, J. Huang, B.Y. Liaw, V. Metzler, J. Zhang, J. Power Sources 254 (2014) 168.
[10] M. Dubarry, B.Y. Liaw, M.-S. Chen, S.-S. Chyan, K.-C. Han, W.-T. Sie, S.-H. Wu, J. Power Sources 196 (2011) 3420.
[11] M. Dubarry, B.Y. Liaw, J. Power Sources 194 (2009) 541.
[12] S. Käbitz, J.B. Gerschler, M. Ecker, Y. Yurdagel, B. Emmermacher, D. André, T. Mitsch, D.U. Sauer, J. Power Sources 239 (2013) 572.
[13] P. Liu, J. Wang, J. Hicks-Garner, E. Sherman, S. Soukiazian, M. Verbrugge, H. Tataria, J. Musser, P. Finamore, J. Electrochem. Soc. 157 (2010) A499.
[14] M. Klett, R. Eriksson, J. Groot, P. Svens, K.C. Högström, R.W. Lindström, H. Berg, T. Gustafson, G. Lindbergh, K. Edström, J. Power Sources 257 (2014) 126.
[15] M. Ecker, N. Nieto, S. Käbitz, J. Schmalstieg, H. Blanke, A. Warnecke, D.U. Sauer, J. Power Sources 248 (2014) 839.
[16] M. Safari, C. Delacourt, J. Electrochem. Soc. 158 (2011) A1123.
[17] A.K. Padhi, K.S. Nanjundaswamy, J.B. Goodenough, J. Electrochem. Soc. 144 (1997) 1188.
[18] I. Bloom, A.N. Jansen, D.P. Abraham, J. Knuth, S.A. Jones, V.S. Battaglia, G.L. Henriksen, J. Power Sources 139 (2005) 295.
[19] A.H. Thompson, J. Electrochem. Soc. 126 (1979) 608.
[20] M. Dubarry, V. Svoboda, R. Hwu, B.Y. Liaw, Electrochem. Solid State Lett. 9 (2006) A454.
[21] M.C. Smart, B.V. Ratnakumar, J. Electrochem. Soc. 158 (2011) A379.
[22] B.V. Ratnakumar, M.C. Smart, ECS Trans. 25 (2010) 241.
[23] M. Petzl, M.A. Danzer, J. Power Sources 254 (2014) 80.
[24] M. Winter, J.O. Besenhard, M.E. Spahr, P. Novák, Adv. Mater. 10 (1998) 725.
[25] N. Legrand, B. Knosp, P. Desprez, F. Lapicque, S. Raël, J. Power Sources 245 (2014) 208.
[26] J. Christensen, J. Newman, J. Electrochem. Soc. 152 (2005) A818.
[27] D. Aurbach, J. Power Sources 89 (2000) 206.
[28] S.J. Harris, A. Timmons, D.R. Baker, C. Monroe, Chem. Phys. Lett. 485 (2010) 265.
[29] B. Bitzer, A. Gruhle, J. Power Sources 262 (2014) 297.
[30] S.-P. Kim, A.C.T. van Duin, V.B. Shenoy, J. Power Sources 196 (2011) 8590.